Published by
NIGERIAN SOCIETY OF PHYSICAL SCIENCES
Available online @ https://journal.nsps.org.ng/index.php/jnsps

J. Nig. Soc. Phys. Sci. 5 (2023) 1140

Journal of the Nigerian Society of Physical Sciences

Unsteady Prandtl nanofluidic flow through stretching sheet due to mixed convection, first-order slip, and chemical reaction

V. Ramanjini[a], G. Gopi Krishna[b,*], Mani Ramanuja[b], Hari Kamala Sree[c], S. R. Mishra[d]

[a]*Department of Mathematics, Government First Grade College Manvi, Raichur - 584123, Karnataka, India*
[b]*Department of Mathematics, Marri Laxman Reddy Institute of Technology and Management, Dundigal, Hyderabad – 500 043, India*
[c]*Department of H & S, Malla Reddy College of Engineering & Technology - 500100, India*
[d]*Department of Mathematics, Siksha 'O' AnusandhanDeeed to be University, Bhubaneswar - 751030, Odisha, India*

Abstract

This article explores the unsteady flow, heat, and mass transport of a Prandtl nanofluid flow over a stretching sheet due to the existence of mixed convection, first-order slip, and chemical reaction. The flow characteristics are analysed for the interaction of thermal and solutal Biot numbers. The system of coupled non-linear leading partial differential equations (PDEs) is converted into non-linear ordinary differential equations (ODEs) with the facilitation of given similarity transformations. Furthermore, these equations are solved by applying a semi-analytical method termed the "*Optimal Homotopy Analysis Method*" (OHAM) using the computational software MATHEMATICA. The tables and figures present the numerical computations of the pertinent parameters of the flow problems. The essential findings of this study are for the growing values of the Prandtl parameter, the velocity profile is enhanced, and the temperature profiles show the opposite behaviour. Unsteady parameters reduced the thickness of the heat and moving boundary layers. The temperature profiles are enhanced as the thermal Biot number grows, and similar characteristics can be observed in the solutal Biot number on concentration profiles.

DOI:10.46481/jnsps.2023.1140

Keywords: Unsteady flow, Prandtlnanofluid, Thermal and solutal Buoyancy conditions, OHAM

Article History :
Received: 22 October 2022
Received in revised form: 30 January 2023
Accepted for publication: 19 April 2023
Published: 08 October 2023

Communicated by: T. Latunde

1. Introduction

The exploration of boundary layer flow over an expanding sheet has been used for decades in the existence of magneto-hydrodynamics (MHD), which plays a significant role in engineering and science. However, the problems involved with those are generally relating to heat and mass transfer phenomena. These developments include the manufacturing procedures like the design of nuclear reactors, cooling processes of a stretching sheet in glass and polymer industries, wire drawing, machine devices, automotive engines, paper production, etc. Due to these industrial applications, many researchers have gained more interest on stretching sheet with fluids having various physical characteristics. The boundary layer behavior over laminar and turbulent flows on a continuous flat plate and solid surfaces was initiated by Sakiadis [1, 2]. Tsou *et al.* [3] studied the continuously expanding surface by unvarying velocity. Crane [4] explored an excellent work on two-dimensional flow of boundary layer more than a stretching sheet. Further, several researchers have designed the Newtonian vis-à-vis non-

*Corresponding author: Tel.: +91-9848206694
Email address: drgopikrishnag@gmail.com (G. Gopi Krishna)

Newtonian fluid past a linear/nonlinear expanding sheets [5–9].

In recent years, research work has shown that base fluids like water, engine oil, ethylene glycol, and grease contain low thermal conductivity in comparison to the metals. To lead this situation, the researchers introduced nanometer-sized metallic particles and then significantly added them to base liquids. As a result, thermo-physical properties improve continuously. Later, these are known as nanofluids, which are created up of tiny minute particle suspensions having a size between 10nm and 50 nm. Best examples of these fluids are metals like, Au, Cu, Ag, oxides$_{Al_2O_3,CuO}$carbide ceramics,$_{Tic,Sic,}$ carbon nanotubes and so on. This concept was a new kind of heat transfer medium that attracted several researchers due to their tremendous utilization in engineering fields and science, a few of them mentioned as chemical production, micro-electronic cooling, air conditioning, transportation, ventilation, and so on. Choi & Eastman [10] was one of the first researchers who worked on nanofluids. The conductivity of the fluids at the usual temperature was experimentally studied by Chon and Kihm [11] and Li and Peterson [12]. Buongiorno [13] has investigated that the Brownian motion and thermophoresis influences are two extensive forces that cause the (slip velocity) drift-flux of nanoparticles in the base fluid. The accurate solution of Cassonnanofluid above permeable shrinking/stretching sheets without and with the extraneous Lorentz force was considered by Krishnendu *et al*. [14]. Prasad *et al*. [15] interpret the enforce of the flux model considering Williamson-Nanofluid flow through an expanding sheet under variable thickness. Recently, Tlili and Tawqeef [16] discussed the nanotechnology for water purification: electrospunnanofibrous membrane in water and waste water treatment. Dadheech *et al.* [17] characterized the Marangoni convection flow of γ–Al2O3 nanofluids past a porous stretching surface with thermal radiation effect in the presence of an inclined magnetic field. Mfon *et al.* [18] studied the impact of biochemical synthesis, characterization, and electrodeposition of silver nanoparticles on a gold substrate. Tlili *et al.* [19, 20] and Hejazi *et al*. [21] explored the inclined surface slip flow of nanoparticles with subject to mixed convection phenomenon and molecular dynamic study of vacancy defect influence on carbon nanotubes.

Nowadays, mixed convection problems have attracted various scientists and researchers owing to its important submission in industries as well as engineering, namely, fans used in various devices, solar receivers, drying technologies, and so on. Keeping an eyes on these applications, Moutsoglou and Chen [22] designed the special possessions of buoyancy on the continuously moving surface. Vajravelu [23] investigated the heat transport aspects over an expanding sheet in the existence of cross flow. Magneto buoyancy forces acting on a porous medium with viscous dissipation were in spected by Das *et al*. [24]. Mixed convection nanofluid flow with MHD on a stretching sheet with thermal radiation was studied by Afshraf *et al*. [25, 26]. Recently, Hayat and Nadeem [27] worked on the buoyancy influences on the heat transport of Hematite–water nanofluid by an expanding sheet. Habib *et al*. [28] recently examined the impact of Stephen blowing on the stretching sheet-induced by the movement of nanofluids. Ohaegbue *et al*. [29] discussed the analysis of hydromagnetic double exothermic chemical reactive flow with convective cooling through a porous medium under biomolecular kinetics. Asif *et al.* [30] and Lund *et al*. [31] observed the unsteady flow of fractional fluid between two parallel walls with arbitrary wall shear stress using Caputo–Fabrizio derivative and fractional order-two dimensional magnetohydrodynamics unsteady flow generalized viscous fluid shrinking sheet.

Most of the above-cited researchers studied the effect of steady/unsteadiness, stretching sheet with mixed convection, melting heat of nanofluid, homogeneous–heterogeneous reactions, convective boundary conditions, etc., using various synthetic techniques. Owing to the earlier survey, no research has yet been undertaken on the influences of buoyancy and chemical reaction with convectively heated unsteady Prandtlnanofluid utilizing the optimal homotopy analysis technique. Considering all of these studies, the existing work aims to examine the study of flow, heat and mass transfer description of an unsteady mixed convective Prandtlnanofluid over a stretching sheet using an approximate analytical study as OHAM (see, [32–34]).

Furthermore, Magnetohydrodynamic (MHD) flow over a shrinking sheet and heat transfer with viscous dissipation has been studied by Lund *et al*. [31]. Unidirectional flows of fractional viscous fluids in a rectangular channel are studied by Asif *et al*. [30]. Shoaib *et al*. [35] have examined he three-dimensional Prandtl nanofluid flow model (TD-PNFM) by utilizing the technique of Levenberg Marquardt with back propagated artificial neural network (TLM-BANN). Hejazi *et al*. [21] have examined the role of velocity slip effects for the mixed convection flow of nanofluid endorsed due to an inclined surface. Vaidya *et al*. [36] interpret the blood flow analysis through a non-uniform inclined channel by treating blood as a non-Newtonian Phan-Thien-Tanner (PTT) liquid. Shuai *et al*. [37] discussed the atomic vacancy defect influence on nano pumping performance of CNT structure with the molecular dynamics (MD) method. Alqahtani *et al*. [38] have designed the atomic obstacle size influence on the Hydrogen flow inside a nanochannel.

Recently, Guled *et al.* [39] discussed the OHAM method for finding MHD slip flow and heat transfer of UCM fluid with the effect of suction/injection due to stretching sheet. Ramanjini *et al.* [40] studied the unsteady axisymmetric Williamson nanofluid flow in the presence of mixed convection and thermal radiation by optimal homotopy analysis method (OHAM). Mallikarjun and Umadevi [41] examined the OHAM technique on the MHD Cattaneo-Christov model for a Williamson fluid flow across a wedge with a convective boundary condition.

The novelty arises because of the slip velocity condition as well as the convective conditions for the heat and solutal profile that enriches the flow phenomena with the afore-mentioned subject cited. The comparative analysis with the earlier published results shows the convergence criteria of the proposed methodology. The significant characteristics of the pertinent parameters are presented through Figures and the simulated results for the rate coefficients are also deployed in tabular form.

2. Formation of the Problem

In this study, 2-D unsteady flow phenomena of a Prandtl nanofluid flow through an expanding sheet in the existence of mixed convective, chemical reaction, and first-order slip is considered. In addition to these, thermal and solutal boundary situations are considered. The stretching sheet is situated on a plane surface at $y = 0$ having x-axis vertically upwards. Here the surface is assumed to be impermeable $v = 0$ and the flow is subjected to a transverse magnetic field of strength B_0. Heat transfer characteristics are analyzed by considering the effects of Brownian motion and thermophoresis phenomena. The velocity of the stretching sheet is assumed to be u and v along the Cartesian co-ordinates x, y-direction respectively. A downward gravitational force g is acting on the sheet. The nanoparticle concentration and temperature by the surface of the stretching sheet is defined as C_w and $T_w$respectively. Further, T_∞ it denote ambient temperature and C_∞ indicates the nanoparticle concentration of the sheet. There exist a buoyancy assisting flow above the sheet and buoyancy opposing flow below the sheet (for more details see Figure 1).

In consideration to these assumptions, the flow phenomena for continuity, momentum, energy and nanoparticle concentration are insured as:

$$\frac{\partial u}{\partial x} + \frac{\partial v}{\partial y} = 0. \tag{1}$$

$$\begin{aligned} &\tfrac{\partial u}{\partial t} + u\tfrac{\partial u}{\partial x} + v\tfrac{\partial u}{\partial y} = \nu\tfrac{A}{C_1}\tfrac{\partial^2 u}{\partial y^2} + \nu\tfrac{A}{C_1^3}\tfrac{\partial^2 u}{\partial y^2}\left(\tfrac{\partial u}{\partial y}\right)^2 \\ &-\tfrac{\sigma B^2}{\rho}u + g\beta_T(T - T_\infty) + g\beta_C(C - C_\infty). \end{aligned} \tag{2}$$

$$\begin{aligned} &\tfrac{\partial T}{\partial t} + u\tfrac{\partial T}{\partial x} + v\tfrac{\partial T}{\partial y} = \alpha_1\tfrac{\partial^2 T}{\partial y^2} + \tau\left[\begin{array}{c} D_B\tfrac{\partial C}{\partial y}\tfrac{\partial T}{\partial y} + \\ \tfrac{D_T}{T}\left(\tfrac{\partial T}{\partial y}\right)^2 \end{array}\right] \\ &+\tfrac{Q_0}{\rho c_p}(T - T_\infty) + \tfrac{\mu}{\rho c_p}\left(\tfrac{\partial u}{\partial y}\right)^2. \end{aligned} \tag{3}$$

$$\begin{aligned} &\tfrac{\partial C}{\partial t} + u\tfrac{\partial C}{\partial x} + v\tfrac{\partial C}{\partial y} = D_B\tfrac{\partial^2 C}{\partial y^2} + \tfrac{D_T}{T_\infty}\tfrac{\partial^2 T}{\partial y^2} \\ &-K_1(C - C_\infty). \end{aligned} \tag{4}$$

with respective boundary situations are:

$$\left.\begin{array}{l} u = U + \alpha_2\tfrac{\partial u}{\partial y},\ v = 0,\ -\left(\tfrac{\partial T}{\partial y}\right) = h_T(T_W - T), \\ -D_B\left(\tfrac{\partial C}{\partial y}\right) = h_c(C_w - C) \quad at\ y = 0, \\ u \to 0, T \to T_\infty\ C \to C_\infty \quad as \quad y \to \infty. \end{array}\right\} \tag{5}$$

Here u and v denote the velocity components along the Cartesian co-ordinates x, y-direction respectively, ν denote kinematic viscosity, g be the gravitational force A and C_1 are constants related to Prandtl fluid, ρ is fluid density, σ is electric conductivity, β_T be the coefficient of thermal expansion, and$C$ be the nanoparticle concentration of fluid respectively, β_C concentration expansion coefficient, τ the heat capacity ratio, D_B and D_T Brownian and thermophoretic diffusions respectively, Q_0 is coefficient of heat generation / absorption, μ is dynamic viscosity, K_1 is rate of reaction, K is the thermal conductivity, c_p be the specific heat, α_2 is the velocity slip parameter, h_T and h_C the heat and mass transfer coefficient, T be the temperature, α_1 be the thermal diffusivity.

The involved governing PDE's are transformed in to a set of ODE's through introducing the following transformation.

$$\left.\begin{array}{l} \eta = y\sqrt{\tfrac{c_0}{\nu(1-\delta t)}},\ \psi = \sqrt{\tfrac{c_0\nu}{(1-\delta t)}}xf'(\eta), \\ \theta(\eta) = \tfrac{T - T_\infty}{T_w - T_\infty},\ T_w = T_\infty + \tfrac{c_0\nu}{(1-\delta t)}, \\ \phi(\eta) = \tfrac{C - C_\infty}{C_w - C_\infty} \text{ and } C_w = C_\infty + \tfrac{c_0\nu}{(1-\delta t)}. \end{array}\right\} \tag{6}$$

For the assistance of above modification, the fluid moments along x *and* y direction are provided in the dimensionless form as:

$$\begin{aligned} u &= \partial\psi/\partial y = \tfrac{cx}{(1-\delta t)}f'(\eta), \\ v &= -\partial\psi/\partial y = \sqrt{\tfrac{\nu c}{(1-\delta t)}}f'(\eta). \end{aligned} \tag{7}$$

Taking into account, the similarity transformations and substituting stream function, Eqns. (2) - (5) can be reduced to the following form:

$$\begin{aligned} &\alpha f''' + \beta f''' f^{n2} + ff'' - Mnf' + \lambda_T(\theta + \lambda_c\phi) \\ &-Al\left(f' + \left(\tfrac{1}{2}\right)\eta f''\right) = 0. \end{aligned} \tag{8}$$

$$\begin{aligned} &\theta'' + \Pr\left[f\theta' + Nb\phi'\theta' + Nt\theta' + Ecf^{n2} + \lambda\theta\right] \\ &-\Pr Al\left(\theta + \left(\tfrac{1}{2}\right)\eta\theta'\right) = 0. \end{aligned} \tag{9}$$

$$\begin{aligned} &\phi'' + \left(\tfrac{Nt}{Nb}\right)\theta'' + Lef\phi' - LeKc\phi - \\ &LeAl\left(\phi + \left(\tfrac{1}{2}\right)\eta\phi'\right) = 0. \end{aligned} \tag{10}$$

$$\left.\begin{array}{l} f(\eta) = 0,\ f'(\eta) - \alpha_2 f''(\eta) = 1, \\ \theta'(\eta) + Bi_T = Bi_T\theta(\eta), \\ \phi'(\eta) + Bi_C = Bi_C\phi(\eta) \end{array}\right\} \text{ at } \eta = 0, \tag{11}$$
$$f'(\eta) \to 0, \quad \theta(\eta) \to 0, \quad \phi(\eta) \to 0, \quad \text{as } \eta \to \infty.$$

The governing dimensionless quantities $\alpha, \beta, Mn, \lambda_T, \lambda_C, Pr, A1, Nb, Nt, \lambda, Ec, Le, Kc, \alpha_2, Bi_T,$ and Bi_C, present in the equations above are known as magnetic parameter, Prandtl fluid parameters, thermal and concentration buoyancy parameters, thermophoresis parameters, Brownian motion, heat source/sink, unsteady parameter, the Eckert number, the Lewis number, Prandtl number, velocity slip, chemical reaction parameter, thermal and solutalBiot numbers respectively, which can be defined as follows.

$$\begin{aligned} &\alpha = \tfrac{A}{C_1},\ \beta = \tfrac{A^2c_0^3x^2}{2C_1^3\nu(1-\delta t)^3},\ Mn = \tfrac{\sigma B^2(1-\delta t)}{\rho c_0}, \\ &\lambda_T = \tfrac{gB_T(1-\delta t)^2(T_w - T_\infty)}{c_0^2 x},\ \lambda_C = \tfrac{B_C(C_w - C_\infty)}{B_T(T_w - T_\infty)}, \\ &\Pr = \tfrac{\nu}{\alpha_1},\ Nb = \tfrac{\tau D_B(C_w - C_\infty)}{\nu}, Nt = \tfrac{\tau D_T(T_w - T_\infty)}{\nu T_\infty}, \\ &\lambda = \tfrac{Q_0 x(1-\delta t)}{\rho c_0 c_p},\ Ec = \tfrac{c_0 x}{c_p(T_w - T_\infty)},\ Le = \tfrac{\nu}{D_B}, \\ &Kc = \tfrac{K_1(1-\delta t)}{c_0},\ \alpha_2 = \lambda_1\sqrt{\tfrac{c_0}{\nu(1-\delta t)}}, \\ &Bi_T = \tfrac{h_T}{K}\sqrt{\tfrac{\nu(1-\delta t)}{c_0}} \text{ and } Bi_C = \tfrac{h_C}{D_B}\sqrt{\tfrac{\nu(1-\delta t)}{c_0}}. \end{aligned} \tag{12}$$

2.1. Physical Quantities

The significant engineering quantities, such as mass transfer rate, drag force, heat transfer rate, are computed as follows.

$$\begin{aligned} C_{f_x} &= \tau_w/U_w^2, \quad Nu_x = xq_w/\alpha_1(T_w - T_\infty), \\ Sh_x &= xj_w/D_B(C_w - C_\infty), \end{aligned}$$

Table 1. Values of Nusselt number, Sherwood number and Skin friction, with the computed CPU time (in seconds) for Dissimilar governing variables and for fixed $Bi_C = Bi_T = 1$, at $10th$ approximation.

α_2	Le	λ	Kc	Nt	Nb	λ_C	λ_T	Mn	β	α	$-f''(0)$	$-\theta'(0)$	$\phi'(0)$	CPU time
0.1	0.22	0.1	0.22	0.2	0.2	0.3	0.3	0.1	0.3	0.1	0.8862	0.5101	0.5553	159.65
										0.5	0.7062	0.5407	0.5564	147.96
										0.9	0.6265	0.5593	0.5583	156.10
0.1	0.22	0.1	0.22	0.2	0.2	0.3	0.3	0.1	0.3	0.1	0.8862	0.5101	0.5553	159.65
									0.7		0.8033	0.5190	0.5555	144.09
									1.1		0.7616	0.5250	0.5556	178.72
0.1	0.22	0.1	0.22	0.2	0.2	0.3	0.3	0.1	0.3	0.1	0.8862	0.5101	0.5553	159.65
								0.5			1.1153	0.4768	0.5542	181.29
								0.9			1.3027	0.4508	0.5536	136.20
0.1	0.22	0.1	0.22	0.2	0.2	0.3	0.3	0.1	0.3	0.1	0.8862	0.5101	0.5553	159.65
							0.6				0.5159	0.5625	0.5576	177.85
							0.9				0.0223	0.6128	0.5609	168.45
0.1	0.22	0.1	0.22	0.2	0.2	0.1	0.3	0.1	0.3	0.1	0.9630	0.4978	0.5548	139.40
						0.3					0.8862	0.5101	0.5553	159.65
						0.5					0.8059	0.5237	0.5558	164.20
0.1	0.22	0.1	0.22	0.2	0.2	0.3	0.3	0.1	0.3	0.1	0.8862	0.5101	0.5553	159.65
					0.4						0.8429	0.4148	0.5664	138.24
					0.6						0.8651	0.4620	0.5664	129.22
0.1	0.22	0.1	0.22	0.5	0.2	0.3	0.3	0.1	0.3	0.1	0.8862	0.5101	0.5553	159.65
				1.0							0.8621	0.4613	0.5609	158.86
				2.0							0.8403	0.4145	0.6079	177.31
0.1	0.22	0.1	-0.2	0.2	0.2	0.3	0.3	0.1	0.3	0.1	0.8674	0.5154	0.4133	123.04
			0.5								0.8862	0.5101	0.5553	159.65
			1.0								0.8961	0.5086	0.6312	124.09
0.1	0.22	0.1	0.2	0.5	0.5	0.1	0.2	0.1	0.2	0.2	0.8781	0.5051	0.5530	146.78
											0.8862	0.5101	0.5553	159.65
											0.9007	0.5204	0.5590	159.88
0.1	0.22	0.1	0.2	0.5	0.5	0.1	0.2	0.1	0.2	0.2	0.8864	0.5109	0.5553	162.32
											0.8716	0.4696	0.5642	141.23
											0.8576	0.4304	0.7089	135.21
0.1	0.22	0.1	0.2	0.5	0.5	0.1	0.2	0.1	0.2	0.2	0.8864	0.5109	0.5553	162.32
		0.3									0.8321	0.3812	0.5723	144.21
		0.5									0.7863	0.2875	0.5920	132.44
0.1	0.22	0.1	0.2	0.5	0.5	0.1	0.2	0.1	0.2	0.2	0.8864	0.5109	0.5553	162.32
	0.66										0.8997	0.5107	0.6621	128.32
	0.96										0.9071	0.5101	0.7089	142.40
0.1	0.22	0.1	0.2	0.5	0.5	0.1	0.2	0.1	0.2	0.2	0.8864	0.5109	0.5553	162.32
0.3											0.6241	0.5071	0.5071	135.52
0.5											0.4709	0.5057	0.5528	161.21

Table 2. Comparison of Skin friction coefficient $f''(0)$ for various approximation of α with $Nb = Nt = Ec = Le = \lambda_T = \lambda_C = Kc = Bi_T = Bi_C = \alpha_2 = 0, \alpha = \beta = 0.2, Pr = 1, Mn = 0.1$.

α	Habib *et al.* [28]	Malik *et al.* [8]	Khan *et al.* [9]	Present result
0	-1.8428	-1.8421	-1.8463	-1.8478
1	-1.0100	-1.0089	-1.0041	-1.0012
5	-0.5213	-0.5210	-0.5223	-0.5205
10	-0.4150	-0.4152	-0.4148	-0.4156

where $\tau_w = \nu\left[\frac{A}{C_1}\frac{\partial u}{\partial y} + \frac{A}{6C_1^3}\left(\frac{\partial u}{\partial y}\right)^3\right]$,
$q_w = -\alpha_1\frac{\partial T}{\partial y}$ and $j_w = -D_B\frac{\partial C}{\partial y}$ at $y = 0$.

The dimensionless form can be created using the leading transformations. The following is a reduction of the mass transfer coefficient, skin friction coefficient, and heat transfer coeffi-

cient.

$$Re_x^{1/2} C_{f_x} = \left[\frac{\alpha\beta}{3} f'''^3(0) + \alpha f''(0)\right],$$

$$Re_x^{-1/2} Nu_x = -\theta'(0) \text{ and } Re_x^{-1/2} Sh_x = -\phi'(0),$$

where $Re_x = c_0 x/\nu(1-\delta t)$ is called Reynolds number.

3. Method of Solution of the Problem

In the current article, the leading equations of highly non-linear ODE's (8)–(10) along with relevant boundary conditions (11) are determined by a semi-analytical method, namely "OHAM (*Optimal Homotopy Analysis Method*)" (see references [32–34, 39–41]). The system of OHAM gives the auxiliary linear operators, initial estimates, and base functions of the problem. To acquire the suitable solutions of the governing equations determining the sensible initial observations and linear operating functions based on the boundary conditions.

$$f_0(\eta) = (1+\alpha_2)^{-1}\left(1 - {}^{1}\!/_{e^{\eta}}\right), \quad \theta_0(\eta) = {}^{1}\!/_{e^{\eta}} \text{ and } \phi_0(\eta) = {}^{1}\!/_{e^{\eta}}, \tag{13}$$

$$\mathcal{L}_f = f''' - f'', \ \mathcal{L}_\theta = \theta'' - \theta' \text{ and } \mathcal{L}_\phi = \phi'' - \phi'. \tag{14}$$

3.1. Convergence Criteria

The auxiliary parameters are referred to as convergence control parameters $(h_f, h_\theta, h_\phi) \neq 0$, which are useful for the convergence criteria. As a result, the optimal homotopyanalysis technique (OHAM) provides a suitable method for achieving the convergent solution. The optimized values of h_f, h_ϕ and h_θ, we will illustrate the averaged and total squared.

The auxiliary parameters are referred to as convergence control the parameters $\left(\hbar_f, \hbar_\theta, \hbar_\phi\right) \neq 0$,

$$\left.\begin{aligned} E_n^f\left(h_f\right) &= \tfrac{1}{M+1}\textstyle\sum_{K=0}^{M}\left(N_f\left[f_{[M]}(n_k), \theta_{[M]}(n_k), \phi_{[M]}(n_k)\right]^2\right) \\ E_n^f\left(h_\theta\right) &= \tfrac{1}{M+1}\textstyle\sum_{K=0}^{M}\left(N_\theta\left[f_{[M]}(n_k), \theta_{[M]}(n_k), \phi_{[M]}(n_k)\right]^2\right) \\ E_n^f\left(h_\phi\right) &= \tfrac{1}{M+1}\textstyle\sum_{K=0}^{M}\left(N_\phi\left[f_{[M]}(n_k), \theta_{[M]}(n_k), \phi_{[M]}(n_k)\right]^2\right) \end{aligned}\right\}, \tag{15}$$

and $E_n^t = E_n^f + E_n^\theta + E_n^\phi, \delta y = 0.5, k = 20$.

To reduce these errors, computational software such as Mathematica is utilized for distinct values of n. Here, the observation clarifies that the averaging nearly and the residual errors are reduced, while the approximation improves, this confirming that OHAM successfully exists.

4. Results and Discussion

The similarity transformations (6) - (7) are used to convert the leading coupled non-linear PDE's (2) - (5) into a set of ODE's (8) - (11). The optimal homotopy analysis scheme is then used to solve these ODEs. Computational software, such as Mathematica, is used to solve these differential equations. To inspect the related physical parameters, such as Prandtl fluid parameters, α and β representative. Magnetic paramete Mn thermal buoyancy parameter λ_T, concentration buoyancy parameter λ_C, unsteady parameter $A1$, Brownian motion parameter Nb, Prandtl parameter Pr, thermophoresis parameter Nt, heat source or sink parameter λ, Lewis parameter Le, Eckert parameter Ec,

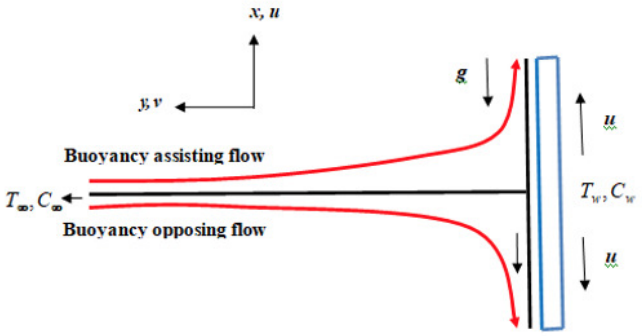

Figure 1. Schematic diagram of Prandtl nanofluid.

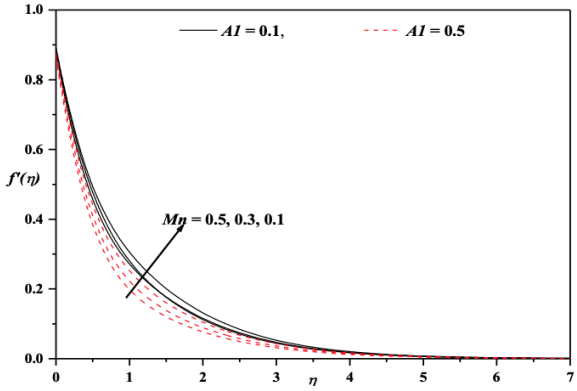

Figure 2. Velocity profile for distinct values of *Al and Mn* with $\alpha = \beta = \lambda_c = \lambda_T = 0.3; \alpha_2 = \lambda = 0.1$ Pr $= Bi_T = Bi_C = 1 Le = 0.22, Nb = Nt = 0.2, Ec = Kc = 0.2$.

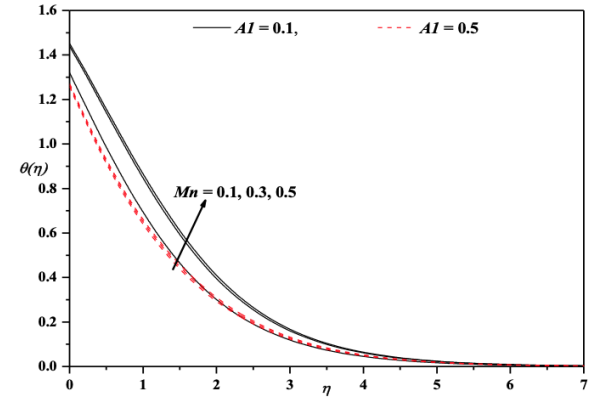

Figure 3. Temperature profile for distinct values of *Al and Mn* with $\alpha = \beta = \lambda_c = \lambda_T = 0.3; \alpha_2 = \lambda = 0.1$ Pr $= Bi_T = Bi_C = 1 Le = 0.22, Nb = Nt = 0.2, Ec = Kc = 0.2$.

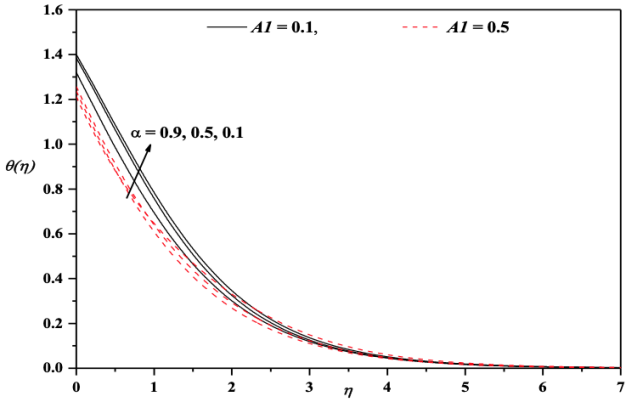

Figure 4. Velocity profile for distinct values of $Al$and $\alpha$with $\beta = \lambda_c = \lambda_T = 0.3$ $Mn = \alpha_2 = \lambda = 0.1$ Pr $= Bi_T = Bi_C = 1$ $Le = 0.22, Nb = Nt = 0.2, Ec = Kc = 0.2$.

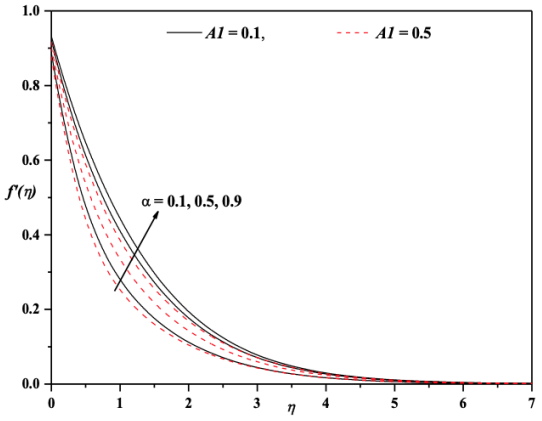

Figure 5. Temperature profile for distinct values of $Al$and $\alpha$with $\beta = \lambda_c = \lambda_T = 0.3$ $Mn = \alpha_2 = \lambda = 0.1$ Pr $= Bi_T = Bi_C = 1$ $Le = 0.22, Nb = Nt = 0.2, Ec = Kc = 0.2$.

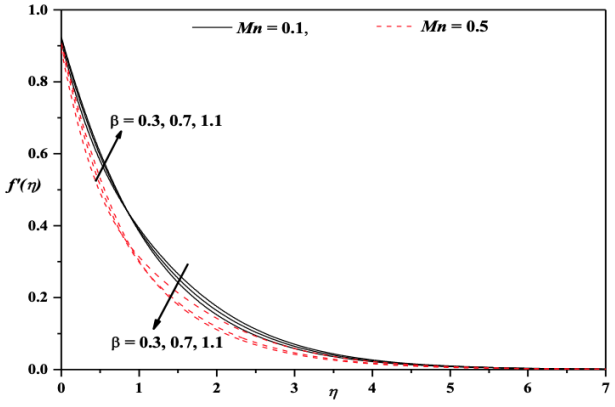

Figure 6. Velocity profile for distinct values of $Mn$and β with$\alpha = \lambda_c = \lambda_T = 0.3$, $Al = \alpha_2 = \lambda = 0.1$ Pr $= Bi_T = Bi_C = 1$ $Le = 0.22, Nb = Nt = 0.2, Ec = Kc = 0.2$.

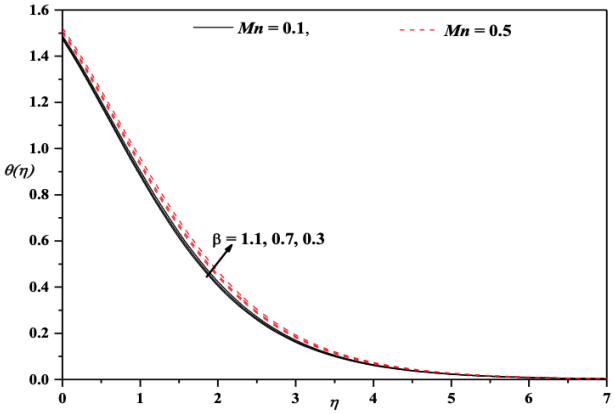

Figure 7. Temperature profile for distinct values of Mn and β with $\alpha = \lambda_c = \lambda_T = 0.3$, $Al = \alpha_2 = \lambda = 0.1$ Pr $= Bi_T = Bi_C = 1$ $Le = 0.22, Nb = Nt = 0.2, Ec = Kc = 0.2$.

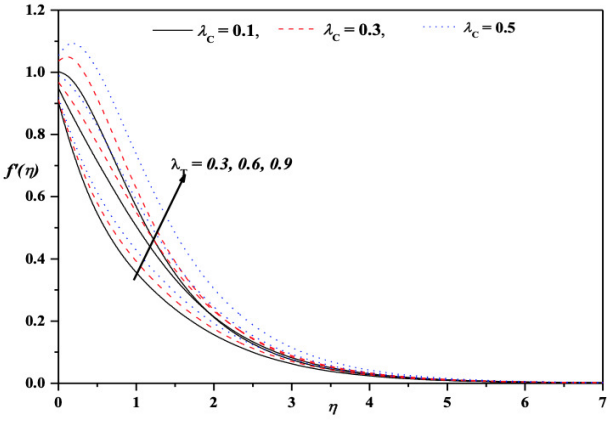

Figure 8. Velocity profile for distinct values of λ_T and $\lambda_T$with $\alpha = \beta = 0.3$, $Mn = \alpha_2 = \lambda = 0.1$Pr $= Bi_T = Bi_C = 1$ $Le = 0.22, Nb = Nt = 0.2, Ec = Kc = 0.2$.

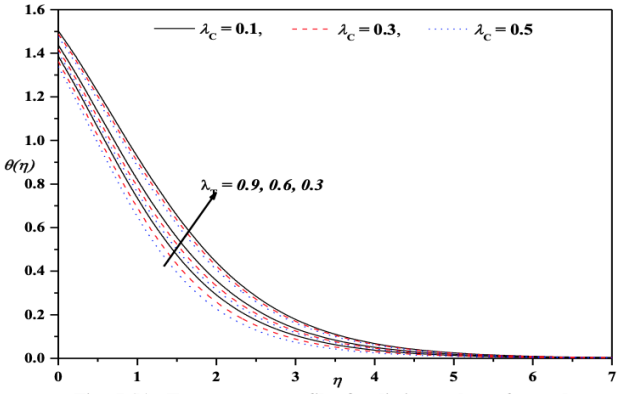

Figure 9. Temperature profile for distinct values of λ_T and $\lambda_T$with $\alpha = \beta = 0.3$, $Mn = \alpha_2 = \lambda = 0.1$Pr $= Bi_T = Bi_C = 1$ $Le = 0.22, Nb = Nt = 0.2, Ec = Kc = 0.2$.

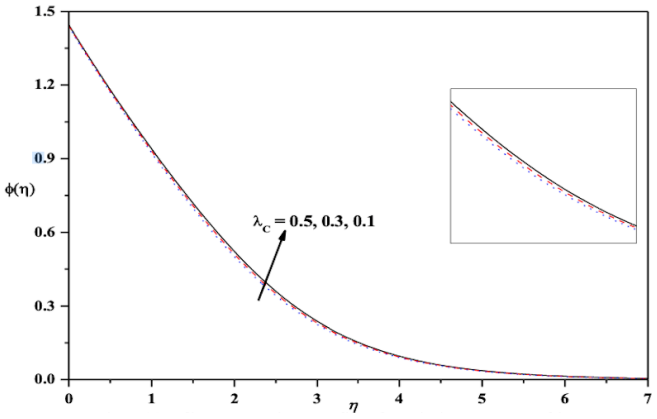

Figure 10. Concentration profile for distinct values of λ_T and $\lambda_T$with $\alpha = \beta = 0.3$, $Mn = \alpha_2 = \lambda = 0.1$Pr $= Bi_T = Bi_C = 1$ $Le = 0.22, Nb = Nt = 0.2, Ec = Kc = 0.2$.

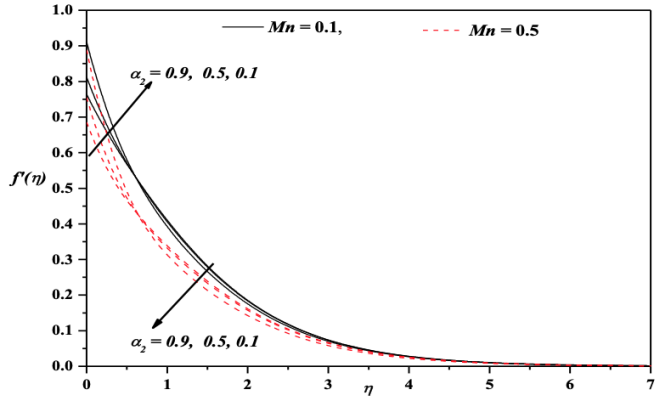

Figure 11. Velocity profile for distinct values ofMn and α_2 with $Al = \lambda = 0.1; \beta = \alpha = \lambda_c = \lambda_T = 0.3,$ Pr $= Bi_T = Bi_C = 1 Le = 0.22, Nb = Nt = 0.2, Ec = Kc = 0.2$.

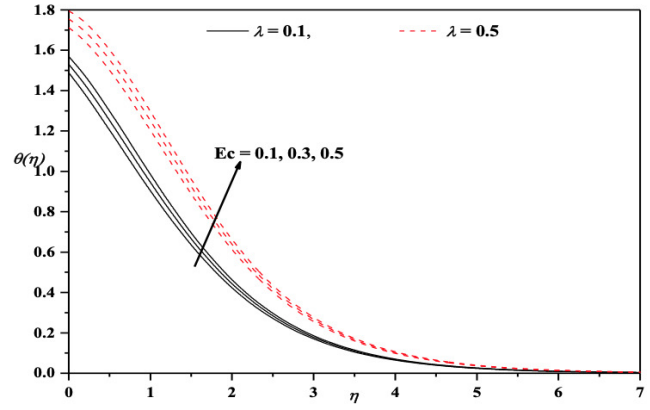

Figure 12. Temperature profile for distinct values of Ec and λ with $Al = \alpha_2 = 0.1, \beta = \alpha = \lambda_T = \lambda_C = 0.3,$ Pr $= Bi_T = Bi_C = 1,$ $Le = 0.22,$ $Nb = Nt = 0.2, Mn = Kc = 0.1$.

$\theta'(0)$ are also studied in detail and dispense in Table 1.

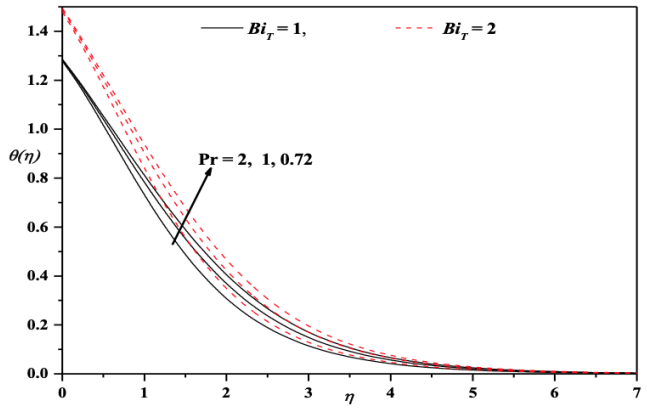

Figure 13. Temperature profile for distinct values of Prand Bi_T with$Al = \lambda = \alpha_2 = 0.1, Le = 0.22 Bi_C = 1, \beta = \alpha = \lambda_T = \lambda_C = 0.3, Mn = 0.1, Nb = Nt = 0.2, Ec = Kc = 0.2$.

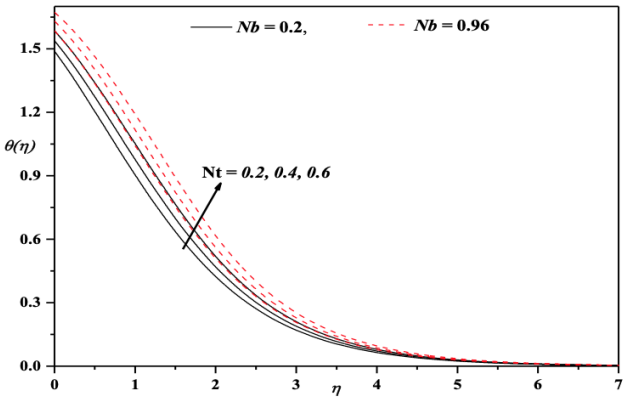

Figure 14. Temperature profile for distinct values of Nb and Nt with $Al = \alpha_2 = \lambda = 0.1, \beta = \alpha = \lambda_T = \lambda_C = 0.3,$ $Mn = Kc = Ec = 0.2,$ Pr $= Bi_T = Bi_C = 1,$ $Le = 0.22$.

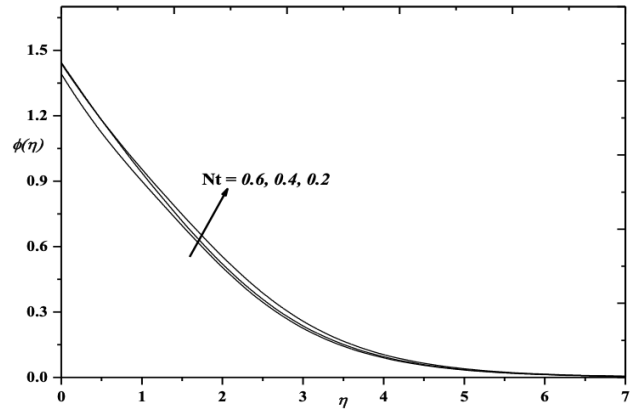

Figure 15. Concentration profile for distinct values of Nt with $Nb = 0.3,$ $Al = \lambda = \alpha_2 = 0.2, \beta = \alpha = \lambda_T = \lambda_C = 0.3,$ $Mn = 0.1,$ $Bi_C =$ Pr $= Bi_T = 1,$ $Le = 0.22,$ $Ec = Kc = 0.2$.

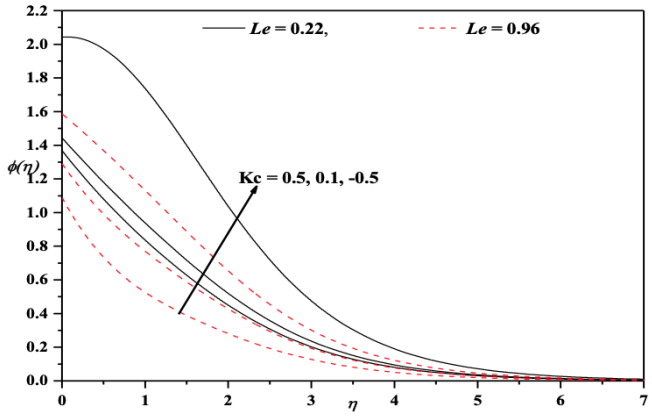

Figure 16. Concentration profile for distinct values of Kc and Le with $Al = \lambda = \alpha_2 = 0.1, \beta = \alpha = \lambda_T = \lambda_C = 0.3$, $Mn = 0.1$, $Bi_C = \Pr = Bi_T = 1$, $Nb = Nt = 0.3$,$Ec = Kc = 0.2$.

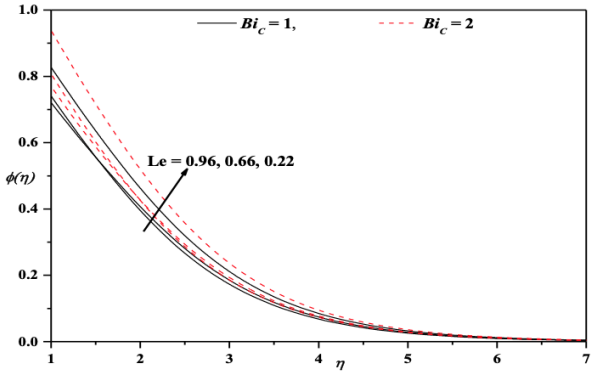

Figure 17. Concentration profile for distinct values of Bi_C and Le with $Al = \lambda = \alpha_2 = 0.1$,$\beta = \alpha = \lambda_T = \lambda_C = 0.3$, $Mn = 0.1$, $\Pr = Bi_T = 1$, $Nb = Nt = 0.3$,$Ec = Kc = 0.2$.

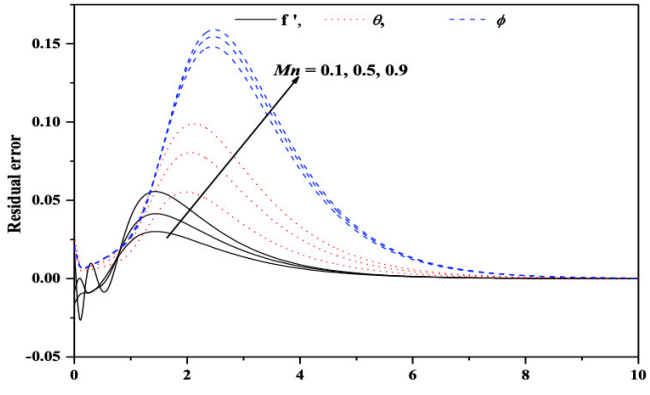

Figure 18. Residual error profiles of velocity, temperature and concentration for distinct values of Mn with $Nb = 0.3$, $Al = \lambda = \alpha_2 = 0.1$,$\beta = \alpha = \lambda_T = \lambda_C = 0.3$, $Bi_C = \Pr = Bi_T = 1$,$Le = 0.22$, $Ec = Kc = 0.2$.

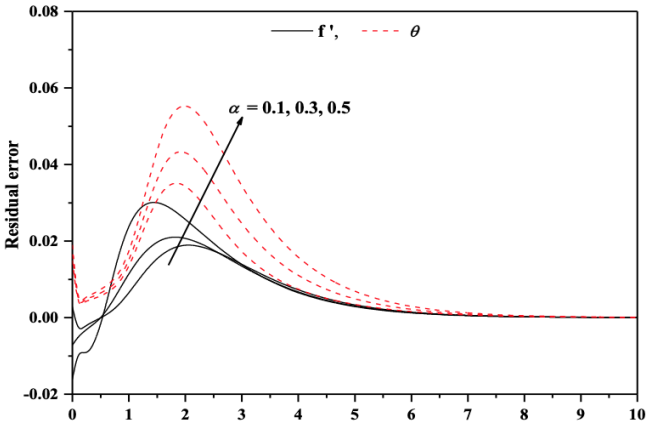

Figure 19. Residual error profiles of velocity and temperature for distinct values of Mn with$Nb = 0.3$, $Al = \lambda = \alpha_2 = 0.1, \beta = \alpha = \lambda_T = \lambda_C = 0.3$, $Bi_C = Pr = Bi_T = 1$, $Le = 0.22, Ec = Kc = 0.2$.

Figure 2 and Figure 3, exhibits the influence of magnetic parameters Mn and unsteady parameter $A1$ over the velocity and temperature profiles. It is clearly shown that $f'(\eta)$decline and $\theta(\eta)$rises for extending values of Mn. In this case, for enhancing values of Mn generate the drag force called the Lorentz force, which acts as drag force reverse to the flowing direction which arises in a decline in rate. In consequence, the thicknesses of the boundary layer momentum diminish as a raise in Mn. The increasing values of unsteady parameter $A1$ decrease the profiles $f'(\eta)$ and $\phi(\eta)$ (see Figure 2 and Figure 3); this is due to the fact that the velocity gradient at the surface is larger for extending values of$A1$. As an effect of the increased skin friction coefficient, the thickness of the boundary layer decreases. Figure 4 and Figure 5 depict the influence of α and $A1$ over $f'(\eta)$ and $\phi(\eta)$. Here observing that $f'(\eta)$ extends and $\theta(\eta)$ reduces as long as higher values of α. Figs. 6 - 7 can be drawn for distinct values of β and Mn. For rising values of β the velocity profiles shows dual nature and temperature profiles decreases. The implication of λ_T and λ_C on profiles is $f'(\eta)$, $\theta(\eta)$ and $\phi(\eta)$ described in Figure 8, Figure 9 & Figure 10, extending values of λ_T a raise in velocity profile $f'(\eta)$ and temperature profile $\theta(\eta)$ decreases. Physically, the λ_T positive values correspond to flow assisting and λ_T negative values results opposite behavior, whereas n$\lambda_T = 0$ signifies then no appearance of buoyancy forces. However, a completely different pattern might noticed in the case of $\theta(\eta)$ and $\phi(\eta)$. Same trend can be reflected for the situation of λ_C. Figure 11 is sketched for various observations of α_2 and Mn on the velocity profile. For extending observations of α_2, it is known that velocity distribution reduces and go on enhanching significantly. Significance of the Eckert number along with heat source/sink on the fluid temperature is dispense in Figure 12 $\theta(\eta)$ enhances as Ec increases and it is appropriate to the relationship between Ec and $(T_w - T_\infty)$, heat source/sink parameter also gives the same pattern. Figure 13 is strained the explanation of dissimilar Pr and Bi_T on temperature profiles $\theta(\eta)$. The fluid temperature enhances as Bi_T extends because Bi_T is pro-

portional to h_T. Suitably stronger convection is occurred due to Bi_T that leads to augment in the profile. Clearly the temperature profile diminishes as larger values of Pr. Clearly, larger Pr shows a greater heat capacity, which strengthen the heat transfer. The influence of Nb and Nt on $\theta(\eta)$ and $\phi(\eta)$ are depicts in Figure 14 and Figure 15. Here inspecting that temperature profiles upgrades whereas concentration distribution declines as long as the values of Nb increases. For Nt, both temperature & concentration profile improves, this is because of the property of thermophoresis that indicated as nano-particles migrate from a hot place to a cooler place, as result $\theta(\eta)$ increases. Figure 16 is drawn for various observations of Lewis parameter Le and Kc over a concentration profile. Higher observations of Le concentration profile decreases, this is because of Le has inverse relation with D_B, which leads to a decline the thickness of the solutal boundary surface. Same effect has seen for the case of Kc. Substantially, $Kc > 0$ shows destructive reaction and whereas $Kc < 0$ gives constructive, and $Kc = 0$ gives null chemical reaction. Figure 17 is plotted for various observations of Le and Bi_C. $\phi(\eta)$ Increases for higher observations of Bi_C, this is because of solutal Biot number is directly proportional to h_C. Figure 18 and Figure 19 give averaged squared residual error graphs for different values of$_{\mathrm{A1,\ Mn\ and}\,\alpha}$. These graphs can be drawn to check the physical behavior and how the residual errors behave with the particular parameters while applying OHAM.

4.1. Physical Parameters Effect on $-f''(0)$, $-f'(0)$ and $-\theta'(0)$

The consequence of different Skin friction coefficient physical parameters $-f''(0)$, Sherwood number and Nusselt number $\theta'(0)$ and $\phi'(0)$ are numerically presented in Table 1. The shear rate reduces for upper values of Mn, Al and enhances for α, λ_T, λ_C and the remaining parameters doesn't show any effect. $\theta'(0)$ enhances for higher observations of Mn, λ, Ec, Nb, Nt, Bi_T and declines for A1, Q, λ_T, λ_C, Pr, and there is no effect for the remaining parameters. In the similar way, $\phi'(0)$ falls for larger observations of λ_C, A1, Le, Kc and enhances for Nb, Nt, Bi_C. Concentration will not affect other parameters.

4.2. Comparison Results of the Work

Here, comparing the results with the earlier published results of Habib *et al.* [22], Malik *et al.* [8] and Khan *et* al. [9] for dissimilar iterations of the Prandtl parameter α on the skin friction coefficient $-f''(0)$ the numerical results are presented in Table 2. The rest of the parameters should be fixed at certain appropriated values. Obtained numerical results are approximately the same as the present work and hence confirm the current work.

5. Conclusions

In this section, we analyzed the influence of unsteady Prandtl nanofluid flow above a stretching sheet due to the interaction of first-order slip and chemical reaction along with thermal and solutalBiot influence. The significant contribution of the leading physical parameters is exhibited by graphs and tables. With the help of these results, the important key points of this work can be written as:

- The fluid velocity vis-a-vis fluid temperature reduces for increasing the values of unsteady parametersA1.
- The rising values of $_{\beta}$ the rate profiles initially reduce and then extend, but the temperature profiles decrease.
- For higher values of buoyancy parameters (both thermal and concentration buoyancy parameters), the velocity profile raises, and opposite results are produced in the fluid temperature.
- For higherα_2, the fluid velocity decrease and gradually increase as away from the sheet.
- The fluid temperature enhances for rising values of Eckert number, and the same behavior can be noticed in the case of$_{\lambda}$.
- The temperature profiles improve for higher values of thermal Biot number. SolutalBiot number also shows the same result.
- Concentration profiles reduce for higher values of$_{Kc}$.

References

[1] B. C. Sakiadis, "Boundary layer behavior on a continuous solid surface: I. Boundary layer equations for two dimensional and axisymmetric flow", Amer. Inst. Ch. Eng. J. **7** (1961) 26. https://doi.org/10.1002/aic.690070108

[2] B. C. Sakiadis, "Boundary layer behavior on a continuous solid surface: II. The boundary layer on a continuous flat surface", Amer. Inst. Ch. Eng. J. **7** (1961) 221. https://doi.org/10.1002/aic.690070211

[3] F. K. Tsou, E. M. Sparrow & R. J. Goldstain, "Flow and heat transfer in the boundary on a continuous moving surface", Int. J. Heat Mass Transf. **10** (1967) 219. https://doi.org/10.1016/0017-9310(67)90100-7

[4] L. J. Crane, "Flow past a stretching plate", Journal of Applied Mathematics and Physics (ZAMP) **21** (1970) 645. https://doi.org/10.1007/BF01587695

[5] B. K. Dutta, P. Roy & A. S. Gupta, "Temperature field in flow over a stretching sheet with uniform heat flux", Int. Commun. Heat Mass Trans. **12** (1985) 89. https://doi.org/10.1016/0735-1933(85)90010-7

[6] L. J. Grubka & K. M. Bobba, "Heat transfer characteristics of a continuous stretching surface with variable temperature", J. Heat Transfer. **107** (1985) 248. https://doi.org/10.1115/1.3247387

[7] C. K. Chen & M. I. Char, "Heat transfer of a continuous stretching surface with suction and blowing", ournal of Mathematical Analysis and Applications **135** (1988) 568. https://doi.org/10.1016/0022-247X(88)90172-2

[8] M. Y. Malik, T. Salahuddin, A. Hussain & S. Bilal, "MHD flow of tangent hyperbolic fluid over a stretching cylinder: using Keller box method", Journal of Magnetism and Magnetic Materials **395** (2015) 271. https://doi.org/10.1016/j.jmmm.2015.07.097

[9] N. S. Akbar, A. Ebaid & Z. H. Khan, "Numerical analysis of magnetic field effects on Eyring-Powell fluid flow towards a stretching sheet", Journal of Magnetism and Magnetic Materials **382** (2015) 355. https://doi.org/10.1016/j.jmmm.2015.01.088

[10] S. U. S. Choi & J. A. Eastman, *Enhancing thermal conductivity of fluids with nanoparticle*, In D. A. Siginer and H. P. Wang (Eds.), Developments and Applications of Non-Newtonian Flows, ASME, New York, Vol. 66, 1995, pp. 99-105. https://ecotert.com/pdf/196525_From_unt-edu.pdf

[11] C. H. Chon & K. D. Kihm, "Thermal conductivity enhancement of nanofluids by Brownian motion", J. Heat Transfer. **127** (2005) 810. https://doi.org/10.1115/1.2033316

[12] C. H. Li & G. P. Peterson, "Experimental investigation of temperature and volume fraction variations on the effective thermal conductivity of nanoparticle suspensions (nanofluids)", J. Appl. Phys. **99** (2006) 084314. https://doi.org/10.1063/1.2191571

[13] J. Buongiorno, "Convective transport in nanofluids", J. Heat Transfer. **128** (2006) 240. https://doi.org/10.1115/1.2150834

[14] B. Krishnendu, H. Tasawar & A. Ahmed, "Analytic solution for magneto hydrodynamic boundary layer flow Casson fluid over a stretching/shrinking sheet with wall mass transfer", Chin. Phy. B. **22** (2013) 522. https://doi.org/10.1088/1674-1056/22/2/024702

[15] K. V. Prasad, V. Hanumesh, K. Vajravelu & V. Ramanjini, "Analytical study of Cattaneo-Christov heat flux model for Williamson-nanofluid flow over a slender elastic sheet with variable thickness", J. of Nonofluid. **7** (2018) 583. https://doi.org/10.1166/jon.2018.1475

[16] I. Tlili & T. A. Alkanhal, "Nanotechnology for water purification: electrospun nanofibrous membrane in water and wastewater treatment", J. Water Reuse and Desalination. **9** (2019) 232. https://doi.org/10.2166/wrd.2019.057

[17] P. K. Dadheech, P. Agrawal & A. Sharma, K. S. Nisar & S. D. Purohit, "Marangoni convection flow of γ–AL_2O_3 nanofluids past a porous stretching surface with thermal radiation effect in the presence of an inclined magnetic field", Heat Transfer **51** (2022) 534. https://doi.org/10.1002/htj.22318

[18] R. E. Mfon, J. J. Deshi, Z. Al Amri & J. S. Madugu, "Biochemical synthesis, characterization and electrodeposition silver nanoparticles on a gold substrate", J. Nig. Soc. Phys. Sci. **4** (2022) 796. https://doi.org/10.46481/jnsps.2022.796

[19] I. Tlili, D. Baleanu, S. M. Sajadi, F. Ghaemi & M. A. Fagiry, "Numerical and experimental analysis of temperature distribution and melt flow in fiber laser welding of inconel 625, Int. J. Advanced Manufacturing and Technology **121** (2022) 765. https://doi.org/10.21203/rs.3.rs-982749/v1

[20] I. Tlili, E. M. Barhoumi, P. C. Okonkwo, I. B. Belgacem & M. Zghaibeh, "Optimal sizing of photovoltaic systems based green hydrogen refueling stations case study Oman", Int. J. Hydrogen Energy. **47** (2022) 31964. https://doi.org/10.1016/j.ijhydene.2022.07.140

[21] H. A. Hejazi, M. I. Khan, A. Raza, K. Smida & S. U. Khan, I. Tlili, "Inclined surface slip flow of nanoparticles with subject to mixed convection phenomenon: fractional calculus applications", J. Indian Chemical Society. **99** (2022) 100564. https://doi.org/10.1016/j.jics.2022.100564

[22] A. Moutsoglou & T. S. Chen, "Buoyancy effects in boundary layers on inclined continuous moving sheets", J. Heat Transfer. **102** (1980) 371. https://doi.org/10.1115/1.3244292

[23] K. Vajravelu, "Convection heat transfer at a stretching sheet with suction or blowing", Journal of Mathematical Analysis and Applications **188** (1994) 1002. https://doi.org/10.1006/jmaa.1994.1476

[24] S. Das, R. N. Jana & O. D. Makinde, "Magneto hydrodynamic mixed convective slip flow over an inclined porous plate with viscous dissipation and joule heating", Alex. Eng. J. **54** (2015) 251. https://doi.org/10.1016/j.aej.2015.03.003

[25] M. B. Ashraf, T. Hayat, A. Alsadi & S. A. Shehzad, "Convective heat and mass transfer in MHD mixed convection of flow of Jeffery nanofluid over a radially stretching surface with thermal radiation", J. Cent. South. Univ. **22** (2015) 1114. http://dx.doi.org/10.1007/s11771-015-2623-6

[26] M. B. Ashraf, T. Hayat & A. Alsadi, "Mixed convection flow of Casson fluid over a stretching sheet with convective boundary conditions and hall effect", Boundary Value Problems **2017** (2017)137. https://doi.org/10.1186/s13661-017-0869-7

[27] T. Hayat & S. Nadeem, "The effects of MHD and buoyancy on Hematite water-based fluid past a convectively heated stretching sheet", Neural Comput. & Applic. **31** (2019) 1083. https://doi.org/10.1007/s00521-017-3139-9

[28] D. Habib, N. Salmat, S. Hussain, B. Ali & S. Abdal, "Significance of Stephen blowing and Lorentz force on dynamics of Prandtl nanofluid via Keller box approach", Int. J. Communications in Heat and Mass transfer **128** (2021) 105599. https://doi.org/10.1016/j.icheatmasstransfer.2021.105599

[29] F. O. Akinpelu, R. A. Oderinu & A. D. Ohaegbue,"Analysis of hydromagnetic double exothermic chemical reactive flow with convective cooling through a porous medium under bimolecular kinetics", J. Nig. Soc. Phys. Sci. **4** (2022) 525. https://doi.org/10.46481/jnsps.2022.525

[30] M. Asif, S. U. Haq, S. Islam, T. A. Alkanhal, Z. A. Khan, I. Khan &K. S. Nisar "Unsteady flow of fractional fluid between two parallel walls with arbitrary wall shear stress using Caputo–Fabrizio derivative", Symmetry **11** (2019) 449. https://doi.org/10.3390/sym11040449

[31] L. A. Lund, Z. Omar, S. O. Alharbi, I. Khan & K. S. Nisar, "Numerical investigation of multiple solutions for Caputo fractional-order-two dimensional magnetohydrodynamic unsteady flow of generalized viscous fluid over a shrinking sheet using the adams-type predictor-corrector method", Coatings **9** (2019) 548. https://doi.org/10.3390/coatings9090548

[32] S. Liao, "An optimal Homotopy – analysis approach for strongly nonlinear equations", Commu. Nonlinear Sci. Num. Simu. **15** (2009) 2003. http://dx.doi.org/10.1016/j.cnsns.2009.09.002

[33] T. Fan & X. You, "Optimal homotopy analysis method for nonlinear differential equations in the boundary layer", Numer. Algor. **62** (2013) 337. https://doi.org/10.1007/s11075-012-9587-5

[34] R. A. Van Gorder" Optimal homotopy analysis and control of error for implicitly defined fully nonlinear differential equations", Numer. Algor. **81** (2019) 181. https://doi.org/10.1007/s11075-018-0540-0

[35] M. Shoaib, G. Zubair, M. A. Z. Raja, K. S. Nisar, A.-H Abdel-Aty & I. S. Yahia, "Study of 3-D Prandtl nanofluid flow over a convectively heated sheet: a stochastic intelligent technique", Coatings **12** (2022) 24. https://doi.org/10.3390/coatings12010024

[36] H. Vaidya, K. Prasad, M. I. Khan., F. Mebarek-Oudina, I. Tlili, C. Rajashekhar, S. Elattar., M. I. Khan & S. G. Al-Gamdi, "Combined effects of chemical reaction and variable thermal conductivity on MHD peristaltic flow of Phan-Thien-Tanner liquid through inclined channel", Case Studies in Thermal Engineering **36** (2022) 102214. https://doi.org/10.1016/j.csite.2022.102214

[37] S. Li, S. M. Sajadi, K. A. M. Alharbi, M. El-Shorbagy & I. Tlili, "The molecular dynamics study of vacancy defect influence on carbon nanotube performance as drug delivery system", Engineering Analysis with Boundary Elements **143** (2022) 109. https://doi.org/10.1016/j.enganabound.2022.06.006

[38] A. M. Alqahtani, S. M. Sajadi, A. S. Al-Johani, K. A. M. Alharbi, A. E. S. Ahmed & I. Tlili, "The atomi obstacle size influence on the Hydrogen flow inside a nanochannel: a molecular dynamics approach to predict the fluid atomic arrangements", Engineering Analysis with Boundary Elements **143** (2022) 547. https://doi.org/10.1016/j.enganabound.2022.06.027

[39] C. N. Guled, J. V. Tawade, M. M. Nandeppanavar & A. R. Saraf, "MHD slip flow and heat transfer of UCM fluid with the effect of suction/injection due to stretching sheet: OHAM solution", Heat Transfer **51** (2022) 3201. https://doi.org/10.1002/htj.22444

[40] V. Ramanjini, G. G. Krishna, S. R. Mishra, S. V. S. Kumari & H. K. Sree, "An unsteady axisymmetric Williamson nanofluid over a radially stretching Riga plate in the presence of mixed convection and thermal radiation", Partial Differential Equations in Applied Mathematics **6** (2022) 100456. https://doi.org/10.1016/j.padiff.2022.100456

[41] P. Mallikarjuna & K. B. Umadevi, "Impact of an MHD Cattaneo-Christov model for a Williamson fluid flow across a wedge with a convective boundary condition: Homotopy analysis method", Int. J. Ambient Energy. **44** (2023) 1097. https://doi.org/10.1080/01430750.2022.2162964

Nomenclature

A and C_1 = Constants related to Prandtl fluid.
$A1$ = Unsteady parameter.
B_0 = Magnetic field strength (tesla).
B_T, B_C = Thermal and solutalBiot numbers.
C = Concentration of the stretching sheet.
C_{f_x} = Skin friction.
C_w = Concentration at wall.
c_p = Specific heat at constant pressure ($J\,kg^{-1}K^{-1}$).
C_∞ = Ambient concentration.
D_B = Brownian diffusion coefficient ($kgm^{-1}s$).
D_T = Thermophoresis diffusion coefficient ($kgm^{-1}s\,K$).
Ec = Eckert number.
f = Dimensionless stream function (m^2s^{-1}).
h_T, h_C = Heat and mass transfer coefficients.
$K1$ = Rate of reaction.
Kc = Chemical reaction parameter.
Le = Lewis number.
Mn = Magnetic parameter.
Nb = Brownian motion parameter.
Nt = Thermophoresis parameter.
Pr = Prandtl number.
q = Heat flux per unit area (Wm^{-2}).
Q_0 = Heat generation/ absorption parameter ($Wm^{-3}K^{-1}$).
T = Temperature (K).
T_w = Temperature at wall (K).
T_0 Solid temperature (K).
T_∞ = Ambient temperature (K).
U = Velocity of the radially stretching Riga plate (ms^{-1}).
u, w = Velocity components in the r and z directions (ms^{-1}).
x, y = Cartesian coordinates.

Greek symbols:

α & β = Prandtl fluid parameters.
α_1 = Thermal diffusivity parameter.
δ = Dimensional constant.
η = Similarity variable.
λ = Heat source/sink parameter.
λ_T & λ_C = Thermal and concentration buoyancy forces.
μ = Coefficient of viscosity ($Ns\,m^{-2}$).
μ_∞ = Ambient viscosity parameter.
ν = Kinematic viscosity (m^2s^{-1}).
ϕ = Dimensionless concentration.
ρ_∞ = Fluid density (kgm^{-3}).
σ = Electrical conductivity.
ψ = Stream function (m^2s^{-1}).
θ Dimensionless temperature (K).
θ_r = Fluid viscosity parameter ($Pa\,s$).
τ = Effective heat capacity of nanoparticle ($J\,K^{-1}$).

Subscripts

∞ = Condition at infinity.
w = Condition at the wall.

Superscript

'= Differentiation with respect to η.